



Boronic Acid-Based *n*-Type Semiconductor for Electronic Device Application

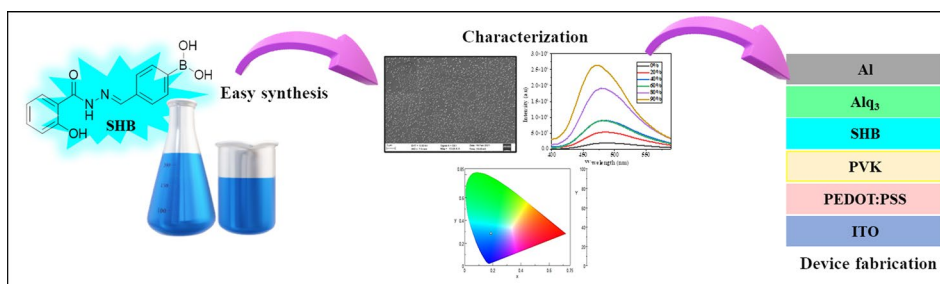
Sneha Kagatkar¹ · Dhanya Sunil¹ · Dhananjaya Kekuda² · M. N. Satyanarayana³ · Suresh D. Kulkarni⁴ · Chaya Karkera⁵

Received: 23 April 2022 / Accepted: 2 August 2022
© The Author(s) 2022

Abstract

Electron transporting, or *n*-type, semiconductors can serve as charge-transport materials, and are ideal for use in organic electronic devices. Boron-based small organic molecules have garnered immense research attention as the heteroatom can effectively alter the electronic structures leading to excellent photophysical and electrochemical properties. A luminescent Schiff base (*E*)-4-((2-(2-hydroxybenzoyl)hydrazono)methyl)phenyl)boronic acid (SHB) was prepared by a one-pot condensation reaction between salicyloyl hydrazide and formylphenylboronic acid. The synthesized molecule was chemically characterized by infrared spectroscopy, nuclear magnetic resonance spectroscopy, and mass spectrometry. The blue-emitting boronic acid-derived molecule displayed intramolecular charge transfer, high carrier concentration, good thermal stability, a reversible reduction tendency and formation of uniform amorphous thin films. A diode was successfully fabricated via a solution processing technique with an ideality factor of 7.76. Further, AC conductivity, dielectric constant, dielectric loss, and capacitance values in a frequency range of 10–1000 Hz were extracted from dielectric studies. The dielectric constant of SHB was found to be 9.71 with an AC conductivity of $6.34 \times 10^{-9} \Omega^{-1} \text{cm}^{-1}$ at 1000 Hz.

Graphical Abstract



Keywords Boronic acid-based Schiff base · *n*-type semiconductor · organic electronics · solution processing · diode

✉ Dhanya Sunil
dhanyadss3@gmail.com

¹ Department of Chemistry, Manipal Institute of Technology, Manipal Academy of Higher Education, Manipal, Karnataka 576104, India

² Department of Physics, Manipal Institute of Technology, Manipal Academy of Higher Education, Manipal, Karnataka 576104, India

³ Optoelectronics Laboratory, Department of Physics, National Institute of Technology Karnataka, Surathkal, Karnataka 575025, India

⁴ Department of Atomic and Molecular Physics, Manipal Academy of Higher Education, Manipal, Karnataka 576104, India

⁵ Department of Nano Science and Engineering, Indian Institute of Science, Bengaluru, Karnataka 560012, India

Introduction

The field of organic electronics using small molecules has garnered much research interest not only due to its unique properties such as highly flexible, conformable, and thin devices, but also being much more economical than conventional inorganic-based electronic devices.^{1,2} Besides, when compared to their polymer counterparts, small-molecule organic semiconductors offer several benefits including well-defined molecular structure, easy functionalization/manipulation of the structural framework to achieve desired functional features, definite molecular weight, and the ability for high-purity synthesis without any batch-wise variation.³ Moreover, the introduction of suitable electron donor and electron acceptor moieties to the molecular scaffold can improve intramolecular charge transfer (ICT), resulting in excellent photophysical properties.⁴ Interestingly, a few small molecules exhibit not only good stability during device fabrication, but also good performance under a wide range of operating conditions.^{5–7}

Boron-based materials have gained significant research attention in recent years as potential candidates in optoelectronic devices.^{8–11} The sp^2 -hybridized electron-deficient boron has only six valence electrons and possesses a vacant low-energy p -orbital that lies orthogonal to the three substituents, which are oriented in a trigonal planar geometry. Hence, materials that incorporate boron generally have rigid/planar molecular structure and usually demonstrate blue photoluminescence with high quantum yield.^{11,12} This environmental friendly molecular system also reveals several unique and attractive properties including high stability, less reactivity, low toxicity, and easy handling.¹³

Boronic acids are organic compounds containing a trivalent boron atom that possess one C-B linkage and two hydroxyl groups appended to boron. Boronate esters are utilized in organic electronic devices.^{14–16} Şimşek reported the preparation of poly(3-thiophene boronic acid) as a semi-conducting polymer for electronic and optical device applications.¹⁷ Kirbiyik et al. described interfacial modifications using boronic acid-functionalized self-assembled monolayers for effective use in inverted polymer solar cells.¹⁸ Kojima and co-workers fabricated organic field-effect transistors using oligomers containing tricoordinated boron atoms.¹⁴ Recently, Choi et al. reported boronic acid-modified alginate conductive hydrogels to improve the physicochemical properties of implantable electronics.¹⁹ Though boronic acid-derived polymer materials have been reported, small-molecule boronic acid derivatives have not been explored as active functional materials in organic electronics to the best of our knowledge.

The development of n -type small-molecule organic semiconductors lags compared to p -type, not only due to

the limited number of highly electron-deficient compact molecular scaffolds that are reported, but also because of their lower solubility in organic solvents.^{20–22} In the present study, a one-pot condensation between 4-formylphenylboronic acid and salicyloyl hydrazide to prepare a boronic acid-derived Schiff base, SHB, is reported. Subsequent to structural characterization, the photophysical, electrical, electrochemical, and surface morphological properties of SHB are investigated. The blue-emitting Schiff base, which displayed an intrinsic n -type semi-conducting behavior is explored for fabricating a diode using a solution-based spin coating technique. Further, the AC conductivity, dielectric constant, dielectric loss, and capacitance are calculated from frequency-dependent dielectric studies.

Materials and Methods

The infrared (IR), nuclear magnetic resonance (NMR), and mass spectra were recorded using Shimadzu Fourier transform infrared (FTIR) and 400 MHz Bruker spectrophotometers and an Agilent 6430 Triple Quad instrument with electrospray ionization, respectively. The absorbance and emission spectra were recorded on 1800 Shimadzu UV–visible and Horiba spectrophotometers. The surface morphological features of thin films were examined using Carl Zeiss EVO 18 analytical scanning (SEM) and INNOVA SPM atomic force (AFM) microscopes. The cyclic voltammetry (CV) measurements were performed using a CH Instrument USA Model 604E series with beta software at a scan rate of 50 mVs^{-1} in a three-electrode conventional cell system using glassy carbon (electroactive area of 0.0771 cm^2) as working electrode, $\text{Ag}/\text{AgCl}(\text{KCl}_{\text{sat}})$ as reference electrode and platinum wire as auxiliary electrode, dipped in 0.1 M tetrabutylammonium hexafluorophosphate in acetonitrile as supporting electrolyte. Electrical measurements were carried out using the Keithley Hall Effect 3706A set-up, the I – V plots were obtained using a Keithley 2400 source meter, and impedance studies were performed using a Hioki LCR meter IM 3635. All the computational studies were carried out using the B3LYP functions of Schrödinger's Materials Science Suite with a 6-31G⁺⁺ basis set in vacuum.

Results and Discussion

Synthesis and Characterization of SHB

4-Formylphenylboronic acid (0.003 mol) and salicyloyl hydrazide (0.003 mol) in ethanol was refluxed for 10 h. The reaction mixture was quenched with water to obtain white precipitate, which was filtered and recrystallized using

ethanol to get the pure product. The synthetic route for SHB is presented in Scheme 1.

(*E*)-4-((2-(2-hydroxybenzoyl)hydrazono)methyl)phenylboronic acid (SHB)-White powder (54.21%) m.p.: 240–242 °C; FT-IR (ATR, cm^{-1}) (Fig. S1): 3248 (O–H *str.*), 1624 (C=O *str.*), 1612 (C=N *str.*), 1359 (B–O *str.*); ^1H NMR (DMSO- d_6 , 400 MHz) (Fig. S2): δ 6.952–6.998 (t, 2H, 8 Hz), 7.436–7.471 (t, 1H, 7 Hz), 7.708–7.727 (d, 2H, 7.6 Hz), 7.872–7.891 (d, 3H, 7.6 Hz), 8.184 (s, 2H, B–OH), 8.470 (s, 1H, CH=N), 11.845 (s, N–H), 11.875 (s, O–H); ^{13}C NMR (DMSO- d_6 , 100 MHz) (Fig. S3): δ 116.43, 117.75, 119.45, 126.67, 129.05, 134.32, 134.98, 135.93, 137.01, 149.21, 159.45, 165.26; MS $\text{C}_{14}\text{H}_{13}\text{O}_4\text{N}_2\text{B}$ (ESI, *m/z*) (Fig. S4): 285.05 ($M+1$).

It is crucial to investigate the absorption and emission features of a material to understand its potential performance in devices. The solid-state electronic spectrum of SHB displayed a broad peak around 310 nm for $\pi - \pi^*$ and 348 nm for $n - \pi^*$ transitions (Fig. 1a). The optical band gap calculated from the Tauc plot (Fig. S5) was 3.71 eV. The solid-state emission spectrum of SHB depicted in Fig. 1b exhibited maximum emission at 478 nm in the blue region with CIE coordinates $x=0.186$ $y=0.283$ (Fig. 1c) and a quantum yield of 1.34. A high Stokes shift value of $11,300 \text{ cm}^{-1}$ for SHB was obtained using Eq. 1, which indicates that there is no reabsorption of radiation.^{23,24} Further, the molar extinction coefficient (ϵ) of SHB, which is the measure of how strongly it can absorb light, was calculated using Eq. 2. The

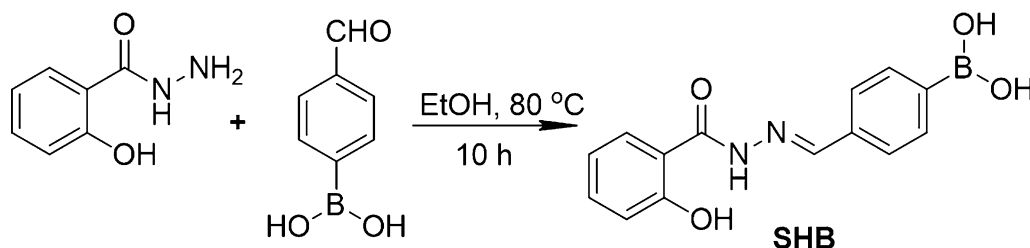
high molar extinction coefficient value of ($\log \epsilon = 6.49$) suggests that the molecule is rigid and the difference between ground and excited states is small with charge transfer through $\pi - \pi$ transitions.²⁵

$$\text{Stokes shift} = \left(\frac{1}{\lambda_{abs}} - \frac{1}{\lambda_{em}} \right) \times 10^7 \quad (1)$$

$$\epsilon = A/mC \quad (2)$$

where A, m and C are absorbance, path length of light and concentration of SHB, respectively.

Furthermore, the electronic distribution of SHB was investigated using density functional theory (DFT) calculations, which was further supported by experimental evidence. The Schrödinger Materials Science Suite software package was used to create the optimized molecular geometry and the molecular orbital (HOMO–LUMO) energy levels of SHB.²⁶ Initially, the stable ground state of SHB was optimized at B3LYP. The optimized geometry and electronic distribution in HOMO and LUMO levels were designed using the 3D model builder and are portrayed in Fig. 2a and b. The electronic distribution of HOMO and LUMO suggests the charge transfer feature in SHB.²⁷ To establish this property, the emission features of about $1 \times 10^{-4} \text{ M}$ solution of SHB in pure THF and different amounts of non-polar hexane ($f_h = 0, 20, 40, 60, 80 \text{ \& } 90\%$) were studied. The emission spectra (Fig. 2c) exhibited not only an obvious



Scheme 1 Schematic representation for the synthesis of SHB.

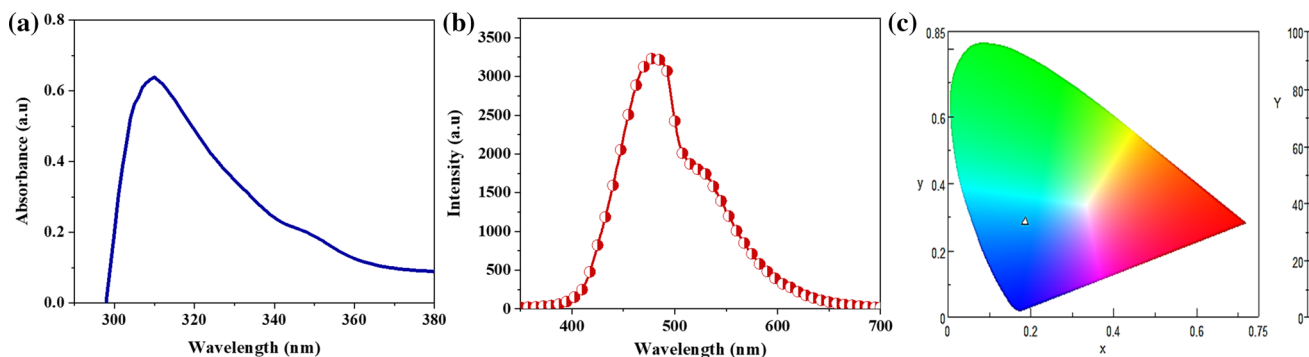


Fig. 1 Solid-state (a) absorption and (b) emission spectra of SHB. (c) CIE coordinates of SHB.

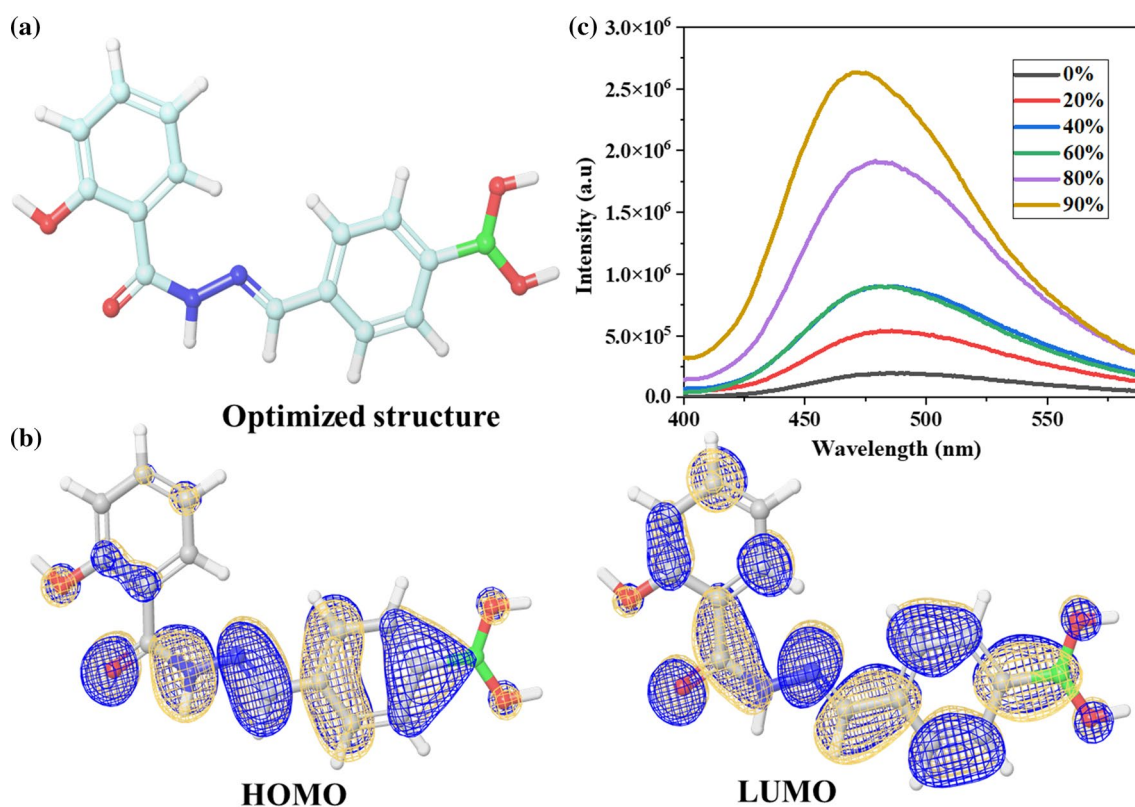


Fig. 2 (a) Optimized geometry and (b) electronic distribution in molecular orbital energy levels of SHB. (c) Emission spectrum of SHB in pure THF and increasing hexane fractions.

increase in emission intensity, but also a hypsochromic shift of ~20 nm with the increase in hexane content, indicating the charge transfer property of SHB. The investigation into the electrical properties of SHB is vital for its plausible application as a functional material in any device. From the Hall effect experiments, SHB was found to be an *n*-type semiconductor with a resistivity of 93.87 Ω cm and mobility of 76.11 cm^2/Vs . A carrier concentration of $8.74 \times 10^{14} \text{ cm}^{-3}$ was also observed for SHB, suggesting its potential use in constructing organic light-emitting devices (OLEDs).

Furthermore, electrochemical studies were carried out to gather deeper insights into the electronic energy levels of SHB, which plays a vital role in device fabrication.²⁸ The values of HOMO and LUMO are associated with redox potentials, which indicates the hole/electron injection capabilities of organic compounds. The current versus voltage plot of SHB as depicted in Fig. 3a shows a redox peak in the positive voltage with a scanning window range of -3.0 to 3.0 V at a scan rate of 50 mVs^{-1} . A reversible reduction system was observed with an oxidation onset at 0.955 eV with a HOMO value of -5.25 eV, reduction onset at 0.776 eV with a LUMO value of -3.52 eV, and an electrochemical band gap of 1.73 eV as calculated using Eqs. 3, 4 and 5, respectively.

$$E_{\text{HOMO}} = -[4.8 - E_{1/2, \text{Fc}/\text{Fc}^+} + E_{\text{oxd}}] \text{ eV} \quad (3)$$

$$E_{\text{LUMO}} = -[4.8 - E_{1/2, \text{Fc}/\text{Fc}^+} + E_{\text{red}}] \text{ eV} \quad (4)$$

$$E_g = E_{\text{LUMO}} - E_{\text{HOMO}} \quad (5)$$

The ability to withstand higher temperatures without undergoing degradation is very crucial for a functional material in devices, where high current can lead to temperature variations. Good thermal features of the active layer can reduce premature device failures and increase the lifetime.²⁹ The variation in the mass of SHB with increasing temperature was examined, and the respective thermogram is presented in Fig. 3b, denoting good thermal stability up to 200°C in concordance with that of previous literature.^{23,30} A two-step degradation process with 10% weight loss observed at 201°C may be attributed to the loss of lattice water molecules, whereas the maximum weight loss of 60.88% detected from 240°C to 496°C can be attributed to the degradation of the molecule.³¹ The high thermal stability of SHB is also an attractive feature

that advocates its candidature as a functional organic semi-conducting material for electronic device fabrication.

The formation of homogeneous thin films with favourable morphological characteristics is yet another desired feature for the fabrication of electronic devices.³² The transport features of a material are strongly associated with the morphology of their films, and therefore must be prudently examined. About 1 wt.% of SHB in THF was spin-coated at 1500 rpm on a cleaned glass substrate to analyse the morphology of the thin films formed. The SEM micrograph presented in Fig. 4a indicates the deposition of pinhole- and crack-free uniform film, which is essential for achieving the desired electrical properties. Moreover, the root-mean-square deviation (R_q) that provides the extent of roughness of the sample was found to be 10.8 nm for SHB. The AFM image as shown in Fig. 4b confirmed the uniform coating, which suggests the feasibility of adopting the solution processing technique for SHB in devices.

Diode: Fabrication and Characterization

Since SHB exhibited good thermal stability, desired carrier concentration, and *n*-type semiconducting behavior, a diode was fabricated; ITO | PEDOT:PSS (~45 nm) | SHB (~100 nm) | Alq₃ (60 nm) | Al, where ITO and PEDOT:PSS acted as the anode and hole transport layer, respectively. SHB was deposited on the spin-coated polymer (2500 rpm) layer. Alq₃ (0.1–0.5 Å/s) and Al (1 Å/s) were deposited through thermal evaporation under vacuum (6×10^{-6} mbar), which served as the electron transport layer and cathode, respectively. The current (*I*) flowed through the system by applying a forward bias of 0–5 V, and the respective *I*–*V* plot is presented in Fig. 5a. It is observed that the current produced in the diode was in microamperes. The ideality factor of the diode calculated using Eq. 6 from the log *I* versus *V* plot (Fig. 5b) was 7.76, which deviated from the ideal diode behavior probably due to the occurrence of interfacial layers and traps, tunnelling or recombination processes, and barrier inhomogeneities.

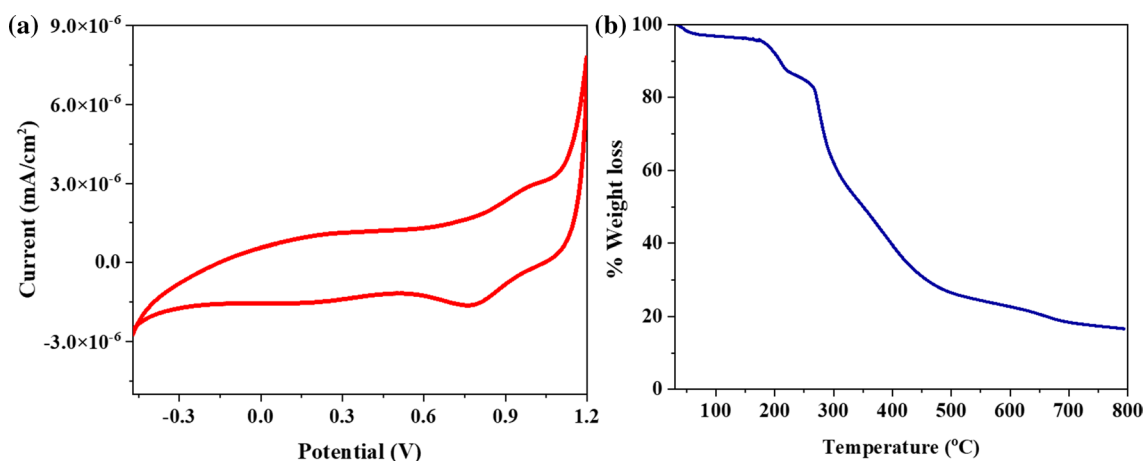


Fig. 3 (a) Cyclic voltammogram and (b) TGA thermogram of SHB.

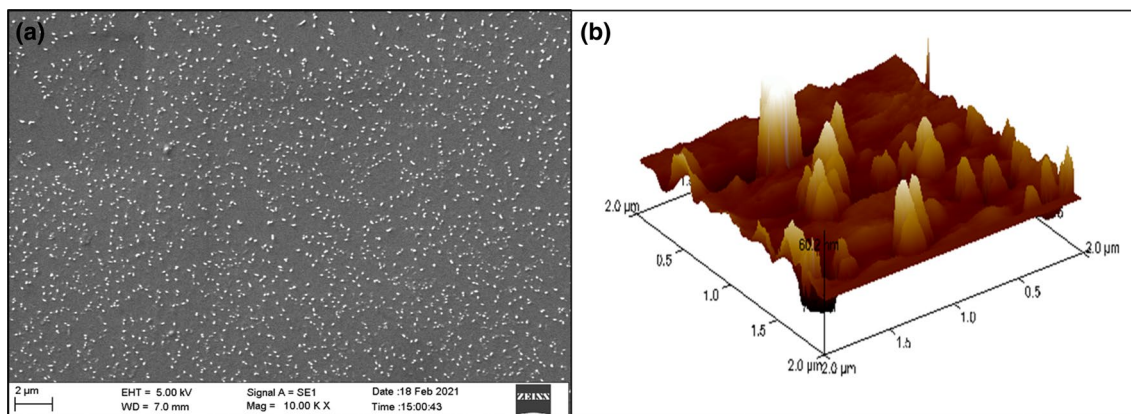


Fig. 4 (a) SEM and (b) AFM images of SHB thin films obtained through spin coating.

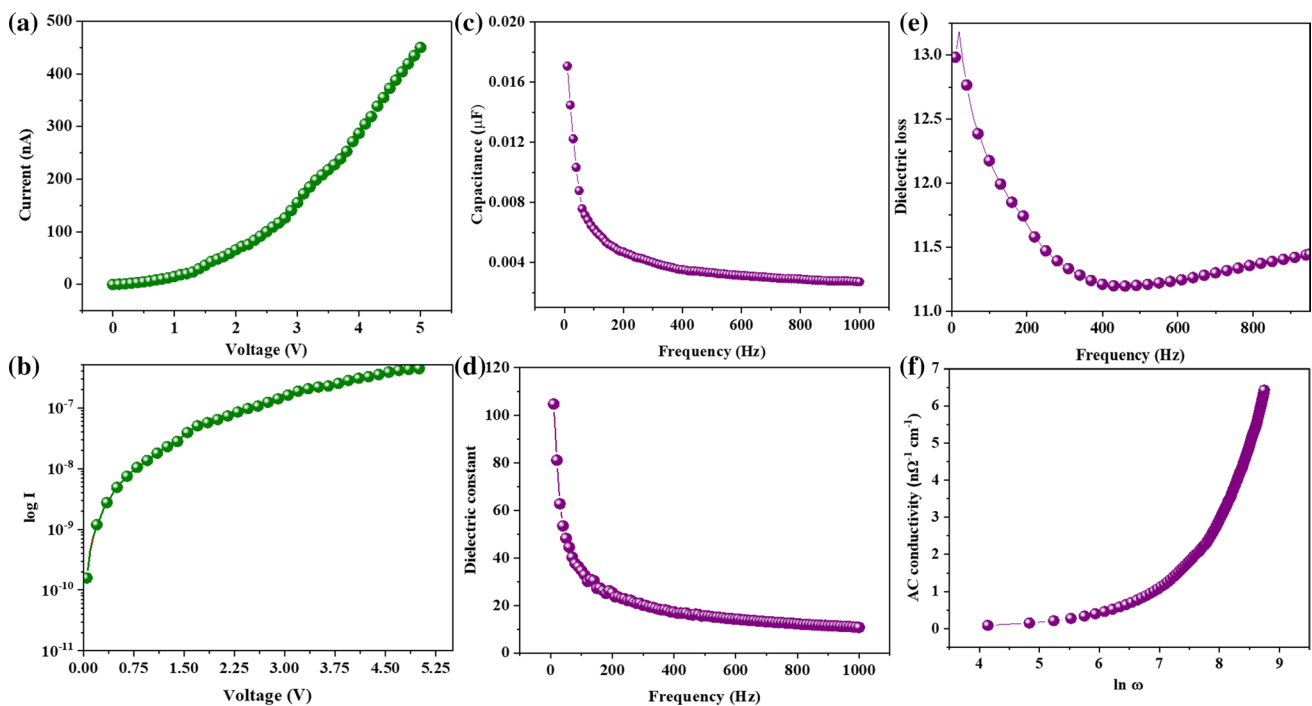


Fig. 5 (a) I–V curve, (b) $\log I$ vs voltage, (c) frequency vs capacitance, (d) dielectric constant vs frequency, (e) dielectric loss vs frequency and (f) frequency-dependent AC conductivity plots of SHB.

$$\eta = \frac{q}{kT} \frac{dV}{d(\log I)} \quad (6)$$

where V , I , q and T are voltage, current, charge and temperature, respectively.

Further, the diode with SHB acted as a parallel-plate capacitor with ITO and Al on either side and the deposited layers as dielectric materials. The frequency-dependent dielectric studies were carried out, and parameters including AC conductivity, dielectric constant, dielectric loss, and capacitance at 10–1000 Hz were extracted. The frequency-dependent capacitance (Fig. 5c) of the system was found to be higher at a lower frequency. A decrease in capacitance was observed with increasing frequency, with a constant capacitance of ~ 3 nF at 1000 Hz. The higher capacitance at a lower frequency might be due to the major carriers, minor carriers, and interfacial states that respond to the lower AC current,³³ and with increasing frequency, some of the minor and interfacial states might be sluggish.³⁴

The dielectric constant, which is the ratio of the permittivity of the system to that of free space is yet another important device parameter. Frequency-dependent dielectric studies were performed (Fig. 5d), and the dielectric constant of the system with SHB as the functional material calculated using Eq. 7 was found to be 9.71 at 1000 Hz. The observed higher value of dielectric constant at low frequencies is due to the effect of space charge polarization. The decreasing trend of the

dielectric constant is ascribed to the inability of the interfacial polarization to respond to the higher frequency.

$$\epsilon_r = \frac{Cd}{\epsilon_0 A} \quad (7)$$

where C , d , ϵ_0 and A are capacitance, thickness, permittivity in the free space and active area of the diode. In adverse conditions including high current and high voltage, the charges flow through the dielectric material causing dissipation of energy, which is referred to as dielectric loss or tangent loss. The frequency-dependent dielectric loss of SHB obtained from the plots (Fig. 5e) was calculated to be 11.81. Generally, the AC conductivity increases the eddy current, which in turn increases the dielectric loss. The AC conductivity obeys the power law which is related to the charge hopping mechanism at the trapped sites. Frequency-dependent AC conductivity (Fig. 5f) was calculated using Eq. 8 and was found to be $6.34 \times 10^{-9} \Omega^{-1} \text{ cm}^{-1}$ at 1000 Hz. The increase in the AC conductivity might be due to the decrease in the series resistance that arises from the dipole–dipole interactions of charges at higher frequencies.³⁵

$$\sigma_{ac} = \omega \epsilon_0 \epsilon_r \tan \delta \quad (8)$$

where ω , ϵ_0 , ϵ_r and $\tan \delta$ are the angular frequency, permittivity in the free space, dielectric constant and dielectric loss, respectively.

Conclusion

The blue-emitting boronic acid-based small-molecule SHB was prepared through an easy condensation reaction between salicyloyl hydrazide and 4-formylphenylboronic acid and was chemically characterized using spectral techniques. The *n*-type semiconductor displayed good optical, electrical, and electrochemical features, thermal stability up to 200°C, and homogeneous film-forming tendency using solution processing. A diode with ITO | PEDOT:PSS | SHB | Alq₃ | Al configuration was fabricated, which exhibited a 7.76 ideality factor with current in microamperes. The device showcased a capacitance of $\sim 3 \times 10^{-9}$ F and a dielectric constant of 9.71 in higher frequencies. The high charge carrier concentration and solution processability feature of the SHB make it a potential candidate for electronic applications, which could be explored further.

Supplementary Information The online version contains supplementary material available at <https://doi.org/10.1007/s11664-022-09864-5>.

Author contributions SK and CK: Methodology, experimental work, preparing the draft manuscript. DS, DK, MNS, and SDK: Conceptualization, supervision, formal analysis, and manuscript editing.

Funding Open access funding provided by Manipal Academy of Higher Education, Manipal. The authors declare that no funds, grants, or other support were received for this work.

Data availability The datasets generated during and/or analyzed during the current study are available from the first author upon reasonable request.

Conflict of interest The authors declare that they have no known competing financial interests or personal relationships that could have appeared to influence the work reported in this paper.

Open Access This article is licensed under a Creative Commons Attribution 4.0 International License, which permits use, sharing, adaptation, distribution and reproduction in any medium or format, as long as you give appropriate credit to the original author(s) and the source, provide a link to the Creative Commons licence, and indicate if changes were made. The images or other third party material in this article are included in the article's Creative Commons licence, unless indicated otherwise in a credit line to the material. If material is not included in the article's Creative Commons licence and your intended use is not permitted by statutory regulation or exceeds the permitted use, you will need to obtain permission directly from the copyright holder. To view a copy of this licence, visit <http://creativecommons.org/licenses/by/4.0/>.

References

- M. Eslamian, Inorganic and Organic Solution-Processed Thin Film Devices. *Nano-Micro Lett.* 9, 1 (2017). <https://doi.org/10.1007/s40820-016-0106-4>.
- M. Fahlman, S. Fabiano, V. Gueskine, D. Simon, M. Berggren, and X. Crispin, Interfaces in Organic Electronics. *Nat. Rev. Mater.* 4, 627 (2019). <https://doi.org/10.1038/s41578-019-0127-y>.
- H. Zhang, X. Wang, L. Yang, S. Zhang, Y. Zhang, C. He, W. Ma, and J. Hou, Improved Domain Size and Purity Enables Efficient All-Small-Molecule Ternary Solar Cells. *Adv. Mater.* 29, 1 (2017). <https://doi.org/10.1002/adma.201703777>.
- G. Forti, A. Nitti, P. Osw, G. Bianchi, R. Po, and D. Pasini, Recent Advances in Non-Fullerene Acceptors of the Idic/Itic Families for Bulk-Heterojunction Organic Solar Cells. *Int. J. Mol. Sci.* 21, 1 (2020). <https://doi.org/10.3390/ijms21218085>.
- Z. Li, Y. Dong, B. Mi, Y. Tang, M. Häußler, H. Tong, Y. Dong, J.W.Y. Lam, Y. Ren, H.H.Y. Sung, K.S. Wong, P. Gao, I.D. Williams, H.S. Kwok, and B.Z. Tang, Structural Control of the Photoluminescence of Silole Regioisomers and Their Utility as Sensitive Regiodiscriminating Chemosensors and Efficient Electroluminescent Materials. *J. Phys. Chem. B.* 109, 10061 (2005). <https://doi.org/10.1021/jp0503462>.
- J.T. Kim, J. Lee, S. Jang, Z. Yu, J.H. Park, E.D. Jung, S. Lee, M.H. Song, D.R. Whang, S. Wu, S.H. Park, D.W. Chang, and B.R. Lee, Solution Processable Small Molecules as Efficient Electron Transport Layers in Organic Optoelectronic Devices. *J. Mater. Chem. A.* 8, 13501 (2020). <https://doi.org/10.1039/d0ta04802j>.
- J. Shao, X. Guo, N. Shi, X. Zhang, S. Liu, Z. Lin, B. Zhao, J. Chang, J. Shao, and X. Dong, Acenaphthylene-imide Based Small Molecules/TiO₂ Bilayer as Electron-Transporting Layer for Solution-Processing Efficient Perovskite Solar Cells. *Sci. China Mater.* 62, 497 (2019). <https://doi.org/10.1007/s40843-018-9337-3>.
- C.D. Entwistle, and T.B. Marder, Applications of Three-Coordinate Organoboron Compounds and Polymers in Optoelectronics. *Chem. Mater.* 16, 4574–4585 (2004). <https://doi.org/10.1021/cm0495717>.
- S.K. Møllerup, and S. Wang, Boron-Doped Molecules for Optoelectronics. *Trends Chem.* 1, 77 (2019). <https://doi.org/10.1016/j.trechm.2019.01.003>.
- U.B. Demirci, P. Miele, and P.G. Yot, Boron-Based (Nano) Materials: Fundamentals and Applications. *Curr. Comput.-Aided Drug Des.* 6, 1 (2016). <https://doi.org/10.3390/cryst6090118>.
- H. Lee, D. Karthik, R. Lampande, J.H. Ryu, and J.H. Kwon, Recent Advancement in Boron-Based Efficient and Pure Blue Thermally Activated Delayed Fluorescence Materials for Organic Light-Emitting Diodes. *Front. Chem.* 8, 1 (2020). <https://doi.org/10.3389/fchem.2020.00373>.
- E. Grotthuss, A. John, T. Kaese, and M. Wagner, Doping Polycyclic Aromatics with Boron for Superior Performance in Materials Science and Catalysis. *Asian J. Org. Chem.* 7, 37 (2018). <https://doi.org/10.1002/ajoc.201700495>.
- M. Elbing and G.C. Bazan, A New Design Strategy for Organic Optoelectronic Materials by Lateral Boryl Substitution. *Angew. Chemie-Int. Ed.* 47, 834 (2008). <https://doi.org/10.1002/anie.200703722>.
- T. Kojima, J.I. Nishida, S. Tokito, and Y. Yamashita, Development of Organic Electronic Devices using Boronate Esters and Related Heterocycles. *Chem. Lett.* 37, 1122 (2008). <https://doi.org/10.1246/cl.2008.1122>.
- S. Park, Z. Liao, B. Ibarlucea, H. Qi, H.H. Lin, D. Becker, J. Melidonie, T. Zhang, H. Sahabudeen, L. Baraban, C.-K. Baek, Z. Zheng, E. Zschech, A. Fery, T. Heine, U. Kaiser, G. Cuniberti, R. Dong, and X. Feng, Two-Dimensional Borate Ester Covalent Organic Framework Thin Film with Large Single Crystalline Domains for a Neuromorphic Memory Device. *Angew. Chemie-Int. Ed.* 59, 8218 (2020). <https://doi.org/10.1002/anie.201916595>.
- N. Keller and T. Bein, Optoelectronic Processes in Covalent Organic Frameworks. *Chem. Soc. Rev.* 50, 1813 (2021). <https://doi.org/10.1039/d0cs00793e>.
- M. Simsek, Electro-Optical Properties of the Perfect Reflector Material: Poly(3-Thiophene Boronic Acid) Semiconducting

- Polymer. *Polym. Eng. Sci.* 56, 707 (2006). <https://doi.org/10.1002/pen.24297>.
18. Ç. Kirbıyık, M. Can, and M. Kuş, Interfacial Modification Via Boronic Acid Functionalized Self-Assembled Monolayers for Efficient Inverted Polymer Solar Cells. *Mater. Sci. Semicond. Process.* 107, 104860 (2020). <https://doi.org/10.1016/j.mssp.2019.104860>.
 19. Y. Choi, K. Park, H. Choi, D. Son, and M. Shin, Self-Healing, Stretchable, Biocompatible, and Conductive Alginate Hydrogels through Dynamic Covalent Bonds for Implantable Electronics. *Polymers (Basel)*. 13, 1133 (2021). <https://doi.org/10.3390/polym13071133>.
 20. K. Feng, W. Shan, S. Ma, Z. Wu, J. Chen, H. Guo, B. Liu, J. Wang, B. Li, H.Y. Woo, S. Fabiano, W. Huang, and X. Guo, Fused Bithiophene Imide Dimer-Based *n*-type Polymers for High-Performance Organic Electrochemical Transistors. *Angew. Chemie - Int. Ed.* 60, 24198 (2021). <https://doi.org/10.1002/anie.202109281>.
 21. J.T.E. Quinn, J. Zhu, X. Li, J. Wang, and Y. Li, Recent Progress in the Development of *n*-type Organic Semiconductors for Organic Field Effect Transistors. *J. Mater. Chem. C*. 5, 8654 (2017). <https://doi.org/10.1039/c7tc01680h>.
 22. O. Toshihiro, K. Shohei, F. Eiji, I. Hiroyuki, W. Go, N. Naoyuki, A. Tatsuro, Y. Masakazu, T. Yukio, S. Hiroki, W. Tetsuya, W. Shun, and T. Jun, Robust, High-Performance *n*-Type Organic Semiconductors. *Sci. Adv.* 6, 427 (2020). <https://doi.org/10.1126/sciadv.aaz0632>.
 23. H. Ulla, M.R. Kiran, B. Garudachari, M.N. Satyanarayan, G. Umesh, and A.M. Isloor, Blue Emitting Halogen-Phenoxy Substituted 1,8-Naphthalimides for Potential Organic Light Emitting Diode Applications. *Opt. Mater. (Amst)* 37, 311 (2014). <https://doi.org/10.1016/j.optmat.2014.06.016.s>.
 24. S. Paşa, Ö. Erdoğan, and Ç. Yenisey, Synthesis and Structural Identification of Boron based Schiff compounds with Ishikawa Endometrial Cancer and Antioxidant Activity. *J. Mol. Struct.* 1186, 458 (2019). <https://doi.org/10.1016/j.molstruc.2019.03.061>.
 25. H. Ulla, B. Garudachari, M.N. Satyanarayan, G. Umesh, and A.M. Isloor, Blue Organic Light Emitting Materials: Synthesis and Characterization of Novel 1,8-Naphthalimide Derivatives. *Opt. Mater. (Amst)* 36, 704 (2014). <https://doi.org/10.1016/j.optmat.2013.11.017>.
 26. L. Segura, C. Seoane, E. Orti, P.M. Viruela, R. Viruela, U. De Valencia, E.-B. Valencia, H. Cano, and J. Veciana, Synthesis, Characterization, and Theoretical Study of Sulfur-Containing Donor-Acceptor DCNQI Derivatives with Photoinduced Intramolecular Electron Transfer. *J. Org. Chem.* 61, 3041–3054 (1996). <https://doi.org/10.1021/jo952274o>.
 27. A. Karuppusamy, T. Vandana, and P. Kannan, Pyrene based Chalcone Materials as Solid State Luminogens with Aggregation- Induced Enhanced Emission Properties. *J. Photochem. Photobiol. A Chem.* 345, 11 (2017). <https://doi.org/10.1016/j.jphotochem.2017.05.026>.
 28. S. Poojary, M. Acharya, A.A. Abdul Salam, D. Kekuda, U. Nayek, S. Madan Kumar, A.V. Adhikari, and D. Sunil, Highly Fluorescent Materials Derived from Ortho-Vanillin: Structural, Photophysical Electrochemical and Theoretical Studies. *J. Mol. Liq.* 275, 792 (2019). <https://doi.org/10.1016/j.molliq.2018.11.067>.
 29. P. He, J. Zhang, J. Zhang, and L. Yin, Effects of Die-Attach Quality on the Mechanical and Thermal Properties of High-Power Light-Emitting Diodes Packaging. *Adv. Mater. Sci. Eng.* (2017). <https://doi.org/10.1155/2017/8658164>.
 30. H. Ulla, M.R. Kiran, B. Garudachari, T.N. Ahipa, K. Tarafder, A.V. Adhikari, G. Umesh, and M.N. Satyanarayan, Blue Emitting 1,8-Naphthalimides with Electron Transport Properties for Organic Light Emitting Diode Applications. *J. Mol. Struct.* 1143, 344 (2017). <https://doi.org/10.1016/j.molstruc.2017.04.103>.
 31. R.G. Chaudhary, H.D. Juneja, and M.P. Gharpure, Thermal Degradation Behaviour of Some Metal Chelate Polymer Compounds with Bis(Bidentate) ligand by TG/DTG/DTA. *J. Therm. Anal. Calorim.* 112, 637 (2013). <https://doi.org/10.1007/s10973-012-2616-8>.
 32. S. Poojary, D. Sunil, D. Kekuda, and S. Sreenivasa, Fluorescent Aromatic Symmetrical Azines: Synthesis and Appraisal of their Photophysical and Electrochemical Properties. *Opt. Mater. (Amst)* 85, 1 (2018). <https://doi.org/10.1016/j.optmat.2018.08.020>.
 33. P. Chattopadhyay and B. RayChaudhuri, Frequency Dependence of Forward Capacitance-Voltage Characteristics of Schottky Barrier Diodes. *Solid State Electron.* 36, 605 (1993). [https://doi.org/10.1016/0038-1101\(93\)90272-R](https://doi.org/10.1016/0038-1101(93)90272-R).
 34. Y. Lee, J. Lee, and J. Park, Dielectric Phenomena of an Organic Light Emitting Diode. *Mol. Cryst. Liq. Cryst. Sci. Technol. Sect. A. Mol. Cryst. Liq. Cryst.* 370, 73 (2001). <https://doi.org/10.1080/10587250108030042>.
 35. K.F. El-Nemr, M.R. Balboul, and M.A. Ali, Electrical and Mechanical Properties of Manganese Dioxide-Magnetite-Filled Acrylonitrile Butadiene Rubber Blends. *J. Thermoplast. Compos. Mater.* 29, 704 (2016). <https://doi.org/10.1177/0892705714533372>.

Publisher's Note Springer Nature remains neutral with regard to jurisdictional claims in published maps and institutional affiliations.